

Production mechanism of neutron-rich transuranium nuclei in $^{238}\text{U} + ^{238}\text{U}$ collisions at near-barrier energies

Kai Zhao,^{1,*} Zhuxia Li,^{1,†} Ning Wang,² Yingxun Zhang,¹ Qingfeng Li,³ Yongjia Wang,³ and Xizhen Wu¹

¹*Department of Nuclear Physics, China Institute of Atomic Energy, P.O. Box 275(10), Beijing 102413, People's Republic of China*

²*Department of Physics, Guangxi Normal University, Guilin 541004, People's Republic of China*

³*School of Science, Huzhou University, Huzhou 313000, People's Republic of China*

(Received 8 February 2015; published 18 August 2015)

The improved quantum molecular dynamics (ImQMD) model incorporated with the statistical evaporation model is applied to study the production mechanism of transuranium nuclei in the reaction of $^{238}\text{U} + ^{238}\text{U}$ at 7.0 MeV/nucleon. The production of primary fragments in the dynamical process is simulated by the ImQMD model, and the decays of them are described by the statistical evaporation model (HIVAP code). The calculated isotope distributions of the residual fragments and the most probable mass number of fragments are generally in agreement with experimental data. By tracking residual fragments back to their original primary fragments with this approach, we find different mechanisms for the production of the residues: the most probable light uraniumlike residues mainly come from the decay of the most probable primary fragments, while the most probable transuranium residues mainly originate from the decay of more neutron-rich primary fragments rather than from the most probable primary ones. For neutron-rich transuranium isotopes $^{254-256}\text{Cf}$, the decay channel of neutron evaporation is suppressed due to the quick drop of the fission barrier height with the increase of neutron number, which leads to the quick drop of the production cross sections for these residues.

DOI: [10.1103/PhysRevC.92.024613](https://doi.org/10.1103/PhysRevC.92.024613)

PACS number(s): 25.70.Lm, 27.90.+b

I. INTRODUCTION

The study of strongly damped reactions between massive nuclei at low energies to synthesize neutron-rich superheavy nuclei (SHN) through multinucleon transfer has experienced a revival of interest experimentally as well as theoretically. This is partly motivated by the fact that the synthesized SHN from $Z = 110$ to 118 using fusion reactions [1–8] are neutron-deficient compared with the center of the predicted first “island of stability” around the neutron number $N = 184$ due to the limitation of the neutron number of available projectiles and targets. In the late 1970s and 1980s there was a great deal of interest in the use of multinucleon transfer reactions with actinide targets to produce new neutron-rich isotopes of heavy and superheavy nuclei. Many such experiments were performed during those times [9–16] and very interesting information concerning collision dynamics was derived. The systematic studies of Zagrebaev and Greiner based on multi-dimensional Langevin equations [17–22] showed the prospect of the production of new neutron-rich isotopes of heavy nuclei and searched for new methods of production of neutron-rich superheavy nuclei by low-energy dissipative collisions of very heavy systems through multinucleon transfer. Stimulated by the importance of this study on the strongly damped reactions between massive nuclei at low energies, a new experiment on the collision of $^{238}\text{U} + ^{238}\text{U}$ at energies between 6.09 and 7.35 MeV/nucleon was performed at the Grand Accélérateur National d'Ions Lourds (GANIL), and the mass distributions of products at several energies were measured [23]. More recently, Kratz *et al.* [24] reexamined data on mass and

charge distributions in collisions of ^{238}U projectiles with thick targets of ^{238}U and ^{248}Cm at near-barrier energies performed at GSI in the 1970s. The cross sections $\sigma(Z)$ below the uranium target were determined as a function of incident energy in thick target bombardments. In addition, the numbers of evaporated neutrons for survival fragments (as well as the excitation energies of primary fragments) were obtained according to the mass differences between the most probable primary fragments and the centroids of the experimental isotope distributions [24–26]. These numbers for the most probable light uraniumlike and heavy transuranium fragments are rather different. However, whether the most probable survival fragments come from the decay of the most probable primary fragments through evaporating neutrons is not clear. And further, how and when the nucleons transfer between projectile and target is also unclear. It seems to us that a microscopic dynamical model study is necessary to understand the mechanism of producing the transuranium fragments and the interplay between the reaction dynamics and the statistical decay in the production process.

Microscopic models such as the time-dependent Hartree-Fock theory (TDHF) and the microscopic transport model have already been used to study the reactions of heavy systems motivated by a large number of degrees of freedom such as those in the excitation and deformation of two nuclei, neck formation, nucleon transfer, different types of separation of the transient composite system and nucleon emission, etc., involved in very heavy system dissipative reactions. The lifetime of the transient composite system for the reaction $^{238}\text{U} + ^{238}\text{U}$ has been calculated, but the production of transuranium and light uraniumlike fragments has not been calculated by the TDHF approach yet [27,28]. The microscopic transport model, i.e., the ImQMD model is an improved version of the quantum molecular dynamics (QMD) model with a series

*zhaokai@ciae.ac.cn

†lizwux@ciae.ac.cn

of modifications aimed at the study of heavy-ion reactions at energies around the Coulomb barrier [29–31]. This model has also been used to study the strongly damped reactions $^{238}\text{U} + ^{238}\text{U}$ and $^{232}\text{Th} + ^{250}\text{Cf}$ [32–35]. The mass distribution of products in $^{238}\text{U} + ^{238}\text{U}$ at 7.0 MeV/nucleon calculated by this model incorporated with the statistical model (HIVAP code) was generally agreement with the experimental measurement of GANIL [23,35]. Further, the orientation effect in the $^{238}\text{U} + ^{238}\text{U}$ reaction at low energies has also been investigated and some interesting results have been obtained [33]. With the newly published experimental results of heavy actinides and their complementary light fragments [24], we conduct this study using the ImQMD model and incorporating the HIVAP code. We first make a comparison of the calculation results with the experimental data to test the validity of the model in the application to the strongly dissipative reaction between very heavy nuclei. Further, we track the residual fragments back to their original primary fragments so that we can precisely know how the residual fragments are obtained from the primary fragments and how many neutrons (or protons or other light particles) are evaporated from the primary fragments. Thus, we can study the different production mechanisms of light uraniumlike fragments and the heavy transuranium isotopes for the most probable and more neutron-rich residual fragments in the reactions between actinide nuclei, which may throw a light on synthesizing the neutron-rich heavy nuclei and the SHN.

The structure of this paper is as follows. In Sec. II, the framework of the ImQMD model is briefly introduced. In Sec. III, the production cross sections for the primary and residual fragments of transuranium and complimentary light uraniumlike nuclei are calculated. The calculation results are compared with the experimental data and calculations from Ref. [24]. Further, the microscopic mechanisms of producing the most probable light uraniumlike residual fragment ^{214}Rn (which is the complementary fragment of Cf), the most probable heavy transuranium residue ^{249}Cf , and the neutron-rich isotopes $^{254-256}\text{Cf}$ are carefully analyzed. Finally, a brief summary is given in Sec. IV.

II. THEORETICAL MODEL

As in the original QMD, each nucleon is represented by a coherent state of a Gaussian wave packet in the ImQMD model. The time evolution of the coordinate and momentum of each nucleon is determined by the mean field part which is described by Hamiltonian equations and the nucleon-nucleon collision part. The Hamiltonian includes the kinetic energy, the nuclear potential energy, and the Coulomb energy. The nuclear potential energy is an integration of the Skyrme-type potential energy density functional, which reads

$$V_{\text{loc}} = \frac{\alpha}{2} \frac{\rho^2}{\rho_0} + \frac{\beta}{\gamma + 1} \frac{\rho^{\gamma+1}}{\rho_0^\gamma} + \frac{g_0}{2\rho_0} (\nabla\rho)^2 + \frac{c_s}{2\rho_0} [\rho^2 - \kappa_s (\nabla\rho)^2] \delta^2 + g_\tau \frac{\rho^{\eta+1}}{\rho_0^\eta}, \quad (1)$$

TABLE I. The model parameters.

α (MeV)	β (MeV)	γ	g_0 (MeV fm ²)	g_τ (MeV)	η	c_s (MeV)	κ_s (fm ²)	ρ_0 (fm ⁻³)
-356	303	7/6	7.0	12.5	2/3	32	0.08	0.165

where $\rho = \rho_n + \rho_p$ is the nucleon density and $\delta = (\rho_n - \rho_p)/(\rho_n + \rho_p)$. ρ_n and ρ_p are the neutron density and the proton density, respectively.

The Coulomb energy in the Hamiltonian is written as a sum of the direct and the exchange contribution:

$$U_{\text{Coul}} = \frac{1}{2} \iint \rho_p(\mathbf{r}) \frac{e^2}{|\mathbf{r} - \mathbf{r}'|} \rho_p(\mathbf{r}') d\mathbf{r} d\mathbf{r}' - e^2 \frac{3}{4} \left(\frac{3}{\pi}\right)^{1/3} \int \rho_p^{4/3} d\mathbf{r}. \quad (2)$$

In the collision term, the isospin-dependent in-medium nucleon-nucleon scattering cross sections are applied, and the Pauli blocking effects are treated as in Ref. [36]. The phase-space occupation number constraint method is adopted in this model. The model parameters are the same as those used in Ref. [33] and are listed in Table I. A more detailed description of the ImQMD model and its applications can be found in Refs. [32,33,35,37,38].

The initial condition of the reaction, such as the properties of projectile and target nuclei, is of vital importance for studying low-energy heavy-ion reactions using the microscopic transport model. In this work, we check the binding energy, the root-mean-square radius, and the deformation of the initial nuclei, as well as their time evolution. The binding energy per nucleon and deformation of ^{238}U are taken as $E_{\text{gs}} = 7.37$ MeV, $\beta_2 = 0.215$, and $\beta_4 = 0.093$ as given by Ref. [39]. In the reactions, only those initially selected nuclei with no spurious particle emission and their properties, such as the binding energy, root-mean-square radius, and deformation being stable within 1000 fm/c, are adopted. The orientations of the initial uranium nuclei in all events are sampled randomly with an equal probability.

In the ImQMD model, the time evolution of the reaction for each event at different incident energies and different impact parameters can be tracked. Both the formation time and the reseparation time of the transient composite system of $^{238}\text{U} + ^{238}\text{U}$ can be recognized in the simulations. The fragments with charge number Z , mass number A , and excitation energy E^* formed in each event can be determined. The cross section of producing this primary fragment with Z , A , and E^* is then calculated by

$$\sigma(Z, A, E^*) = \int_0^{b_{\text{max}}} 2\pi b db \frac{N_{\text{frag}}(Z, A, b, E^*)}{N_{\text{tot}}(b)} = \sum_{b=0}^{b_{\text{max}}} 2\pi b \Delta b \frac{N_{\text{frag}}(Z, A, b, E^*)}{N_{\text{tot}}(b)}. \quad (3)$$

Here b is the impact parameter and $N_{\text{frag}}(Z, A, b, E^*)$ is the number of events in which a fragment (Z, A, E^*) is formed at a given impact parameter b . The excitation energy E^*

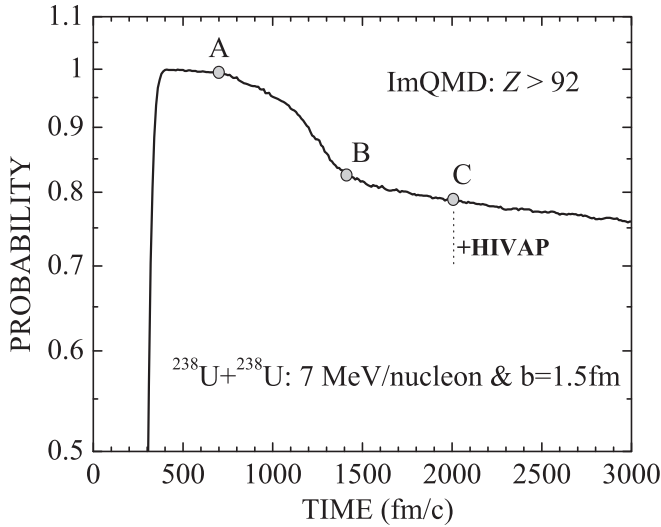


FIG. 1. Time evolution of the production probability for fragments with charge number $Z > 92$ from the ImQMD calculation.

for the fragment with charge number Z and mass number A is obtained by subtracting the corresponding ground-state energy [39] from the total energy of the excited fragment in its rest frame. $N_{\text{tot}}(b)$ is the total event number at a given impact parameter b . The emitting angles of primary fragments can also be obtained, similarly. In this work, the maximum impact parameter is taken to be $b_{\text{max}} = 15$ fm, and the impact parameter step is $\Delta b = 0.15$ fm. The initial distance between the centers of mass of the projectile and the target is taken to be 40 fm. 100 000 events for each impact parameter are simulated in this work.

The survival probability of an excited fragment is calculated using the HIVAP code [40,41] in the subsequent deexcitation process, leading to a final residual nucleus in its ground state. In the deexcitation of primary fragments through evaporation of γ , n , p , and α particles, we assume that the emitting angle of the fragments remains unchanged. We also suppose that the complementary pair fragments share the residual Coulomb energy between them according to their sizes. This energy will eventually contribute to the kinetic energies of the fragments. In the HIVAP code, the successive stages of the deexcitation for the fragment with charge number Z , mass number A , and excitation energy E^* are described by branching ratios expressed by relative partial decay widths for all possible decay modes, $\Gamma_i(Z, A, E^*)/\Gamma_{\text{tot}}(Z, A, E^*)$, where $\Gamma_{\text{tot}}(Z, A, E^*) = \sum_i \Gamma_i(Z, A, E^*)$ and $i = \gamma, n, p, \alpha$, and fission.

To obtain an appropriate matching time that is the time to terminate the ImQMD simulation and to apply the HIVAP code for the description of the decay process of primary fragments, we create 1000 event test runs for $^{238}\text{U} + ^{238}\text{U}$ at 7.0 MeV/nucleon with the impact parameter $b = 1.5$ fm to calculate the time evolution of the average probability of forming a fragment with a charge number of $Z > 92$, i.e., the $P_{Z>92}$. Figure 1 shows the time evolution of the $P_{Z>92}$. One sees from the figure that from time around 300 fm/c to time A, the projectile and the target stick together, i.e.,

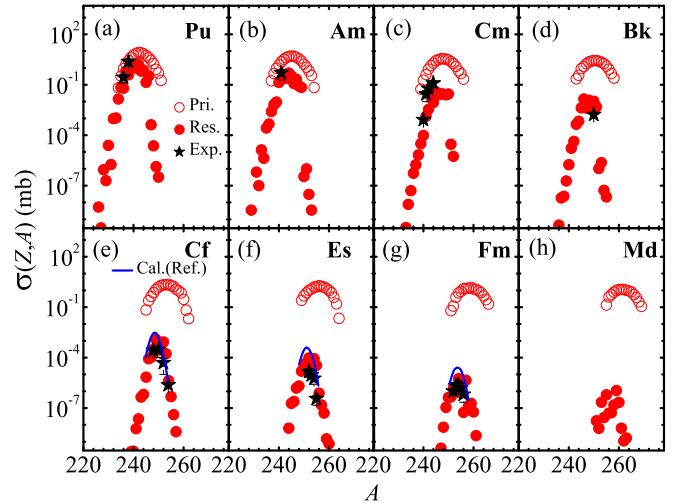


FIG. 2. (Color online) Isotopic production cross sections for transuranium elements from $Z = 94$ to 101. The cross sections for primary fragments and residual fragments are denoted by red open and solid circles, respectively. The experimental data and calculation results from Ref. [24] for Cf, Es, and Fm are shown by black solid stars and blue solid lines, respectively.

the transient composite system is formed and the $P_{Z>92}$ equals 1. From point A to B, the $P_{Z>92}$ decreases quickly due to the quick reparation of the composite system. After time B, the $P_{Z>92}$ decreases with a constant slope, which means the reaction system almost completely enters into the statistical decay stage. We thus take the time of 1000 fm/c after reparation of the composite system as the matching time, which corresponds to point C in Fig. 1. At this time, the dynamical process can be considered to be finished already. The decay of produced primary fragments can be described by the statistical evaporation model. For larger impact parameters, the dynamical process is even faster and the 1000 fm/c after reparation is long enough for the dynamical calculations.

III. RESULTS AND DISCUSSION

In Fig. 2, we present the isotopic production cross sections $\sigma(Z, A)$ for primary (open symbols) and residual fragments (solid symbols) with charge numbers from $Z = 94$ to 101 in the reaction $^{238}\text{U} + ^{238}\text{U}$ at 7.0 MeV/nucleon. For the results shown in this work, an angle cut of $32.5^\circ - 44.5^\circ$ in the laboratory system is taken, the same as that in the experiment [10,24]. The experimental data and calculation results from Refs. [10,24] denoted by black solid stars and blue lines, respectively, are also shown in Fig. 2 for comparison. One can see that the experimental data are generally reproduced, except the mendelevium isotopes ($Z = 101$), which were not yet detected in the experiment. The present calculated cross sections for the most probable residual fragments of Cf, Es, and Fm are slightly larger than the experimental data, but smaller than those of the calculation results from Refs. [10,24]. Comparing the isotope distributions for primary and residual fragments, we find the following three features: the widths of the isotope distributions for residual fragments

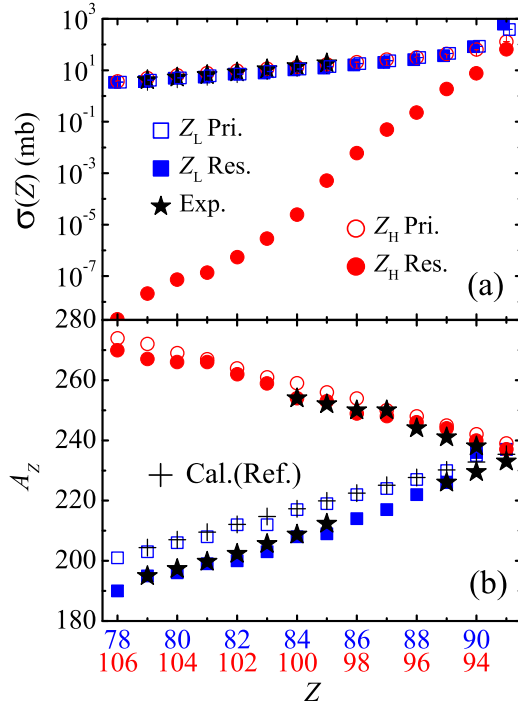


FIG. 3. (Color online) (a) The production cross sections and (b) the most probable mass numbers of primary fragments and residual fragments for complementary elements. The horizontal axis denotes the atomic numbers of complementary elements. Primary and residual fragments are denoted by open and solid symbols, respectively. The transuranium and light uraniumlike nuclei are denoted by red circles and blue squares, respectively. The experimental data and calculation results from Ref. [24] are denoted by black solid stars and cross symbols, respectively.

are much smaller than those for primary fragments for the same element; the peaks in the isotope distributions for residual fragments shift to the less neutron-rich side compared with those for primary fragments; and the production cross sections for the most probable residual transuranium fragments ($Z = 96-101$) decrease almost exponentially with the increase of the fragment charge number.

From the isotopic cross sections $\sigma(Z, A)$ for primary fragments and residual fragments, we can calculate the cross section $\sigma(Z) = \sum_A \sigma(Z, A)$ and the most probable mass number A_Z for the isotope distribution through $\sigma(Z, A_Z) = \max\{\sigma(Z, A)\}$ for each element. In Fig. 3(a), we present the cross section $\sigma(Z)$ for primary fragments (open symbols) and residual fragments (solid symbols). The horizontal axis in Fig. 3 represents the charge numbers of the complementary elements, Z_L and Z_H , where Z_L denotes the charge number of light uraniumlike fragments ($Z < 92$), Z_H denotes that for transuranium fragments ($Z > 92$), and $Z_L + Z_H = 184$. One can see that the experimental data are generally reproduced by our calculation. Moreover, it is shown in Fig. 3(a) that the production cross sections for residual light uraniumlike fragments are close to those for primary fragments, while those for residual transuranium fragments decrease exponentially with the increasing of the atomic number and they are several orders of magnitude smaller than those for the primary

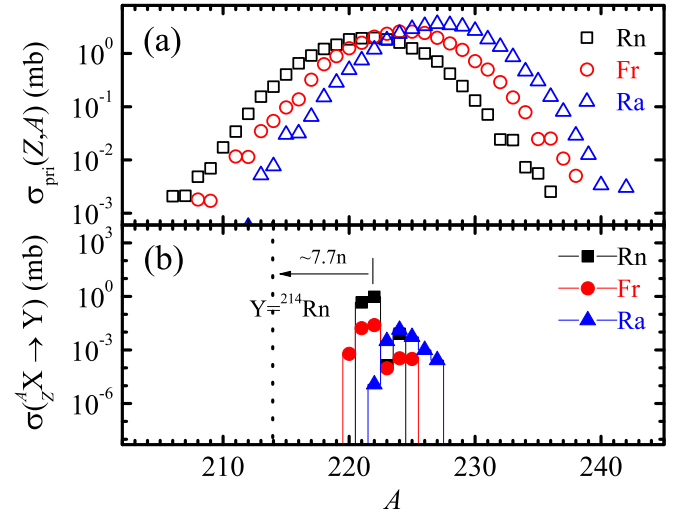


FIG. 4. (Color online) (a) The isotope distributions for primary fragments of Rn, Fr, and Ra and (b) the production cross sections for the residue ^{214}Rn from the decay of primary fragments of Rn, Fr, and Ra, respectively. Here ${}^A_Z X$ denotes the primary fragments X with charge number Z and mass number A . Y represents the evaporation residue.

transuranium fragments. The fission barrier heights for light uraniumlike nuclei are much higher than those for heavy transuranium nuclei so that most of light primary uraniumlike fragments survive fission and heavy transuranium nuclei hardly survive fission (see Fig. 6). Figure 3(b) shows the most probable mass numbers of primary fragments and residual fragments. The experimental data and calculation results from Ref. [24] are also shown for comparison. The experimental maximum isotope cross sections are generally reproduced by our calculations, and the calculated most probable mass numbers for primary light fragments ($Z = 79-91$) generally agree with the model predictions from Ref. [24]. The calculated results indicate that there exists a difference of about five to ten neutrons between the most probable mass numbers of primary fragments and those of residual fragments for light uraniumlike nuclei with $Z < 89$, while this difference is much smaller for transuranium nuclei, which is consistent with the results in Ref. [24].

Now let us study the microscopic mechanism of producing the individual isotopes of the complementary elements Rn and Cf. We first investigate the production mechanism of the most probable light uraniumlike fragment ^{214}Rn . Figure 4(a) shows the isotope distributions of the primary fragments of Rn, Fr, and Ra. The production cross sections for the residue ^{214}Rn from the decay of primary fragments of Rn, Fr, and Ra are shown in Fig. 4(b). One can see from the figure that the isotope distributions for primary fragments of Rn, Fr, and Ra are all of the parabolic shape and the magnitudes of cross sections are similar for the three elements, except that the peak shifts toward larger mass numbers for larger charge number elements. We track the residue ^{214}Rn back to its original primary fragments and find that the most probable residue ^{214}Rn is from the decay of $^{221,222}\text{Rn}$ evaporating seven to eight neutrons, which takes up over 90% of the total yield of residue ^{214}Rn , and also from

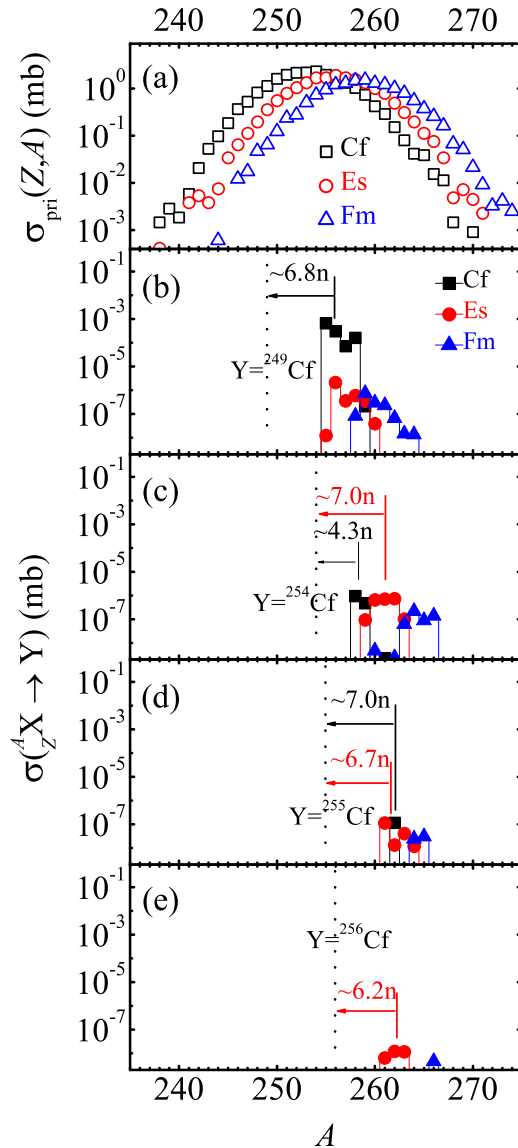


FIG. 5. (Color online) The isotope distributions for primary fragments of Cf, Es, and Fm are shown in panel (a) and the cross sections for the residues ^{249}Cf , ^{254}Cf , ^{255}Cf , and ^{256}Cf contributed from the decay of primary fragments of Cf, Es, and Fm are shown in panels (b)–(e), respectively. The meanings of $^A_Z X$ and Y are the same as in Fig. 4.

$^{221,222}\text{Fr}$ and ^{224}Ra . The production probability of the most probable residue ^{214}Rn is very high due to the high fission barrier of $^{221-222}\text{Rn}$ [see Fig. 6(e)]. The contributions from the decay of primary fragments $^{221-222}\text{Fr}$ and ^{224}Ra , which are at the neutron-deficient side of Fr and Ra isotopes, are minor because the decay channels of evaporating charged particles are suppressed by the Coulomb barrier.

Figure 5 shows the isotope distributions of the production cross sections for primary fragments of Cf, Es, and Fm [panel (a)] and for the most probable residue ^{249}Cf as well as the neutron-rich residues $^{254-256}\text{Cf}$ [panels (b)–(e)], respectively. One can see from Fig. 5(a) that the feature of the isotope distributions for primary fragments of Cf, Es,

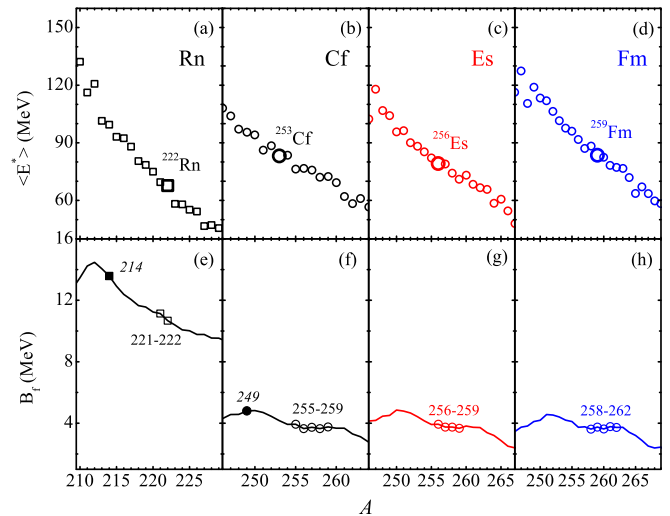


FIG. 6. (Color online) The isotope dependence of the average excitation energies of primary fragments (upper panels) and the fission barrier heights (lower panels) for Rn, Cf, Es, and Fm, respectively. The most probable primary fragments are denoted by larger size symbols in panels (a)–(d). In panels (e)–(h), the most probable residual fragments are denoted by solid symbols, and the primary fragments decaying to the most probable residual fragments are denoted by open symbols in the corresponding panels.

and Fm are similar to those of primary fragments of Rn, Fr, and Ra, but here the cross sections decrease slightly with the increase of the charge number of elements. The isotope distributions of the cross sections for primary fragments shown in Figs. 4 and 5 suggest that a large mass transfer takes place during the dynamical process in the reaction. We also find from the ImQMD model calculations that the primary fragments emitted within the angle of 32.5° – 44.5° are mainly contributed from the reactions at impact parameter region $b = 4$ – 8 fm. Figures 5(b)–5(e) denote the production cross sections for residues $^{249,254-256}\text{Cf}$ from the decay of primary fragments of Cf, Es, and Fm. It can be found that the survival probabilities of heavy transuranium primary fragments are very small. For the most probable residue ^{249}Cf , the cross section is 3 orders of magnitude smaller than that for the most probable residual fragment ^{214}Rn , which is caused by a much lower fission barrier for these transuranium nuclei (see Fig. 6). Similarly, by tracking the residue ^{249}Cf back to its original primary fragments, we find it comes from primary fragments $^{255-259}\text{Cf}$, $^{256-259}\text{Es}$, and $^{258-262}\text{Fm}$. Here, over 90% of ^{249}Cf comes from the decay of the primary fragments $^{255-259}\text{Cf}$ by evaporating six to ten neutrons. We notice that the primary fragments $^{255-259}\text{Cf}$ are about two to six neutrons richer than the most probable primary fragment ^{253}Cf . This is different from the case of the evaporation residue ^{214}Rn , which is mainly produced from the decay of the most probable primary fragments $^{221-222}\text{Rn}$. The cross sections for ^{249}Cf from the decay of primary fragments of Es and Fm are less than 10% because the decay channels of evaporating charged particles are strongly suppressed by the high Coulomb barrier the same as the ^{214}Rn case. For the neutron-rich isotopes $^{254-256}\text{Cf}$, the cross sections are lower down to 10^{-6} – 10^{-8} mb. Only ^{254}Cf

was experimentally observed in the $^{238}\text{U} + ^{238}\text{U}$ reactions (see Fig. 2). Upon looking at Figs. 5(b)–5(e) more closely, one can see that for neutron-rich residues $^{254-256}\text{Cf}$ the contributions from the decay of primary fragments $^{255-259}\text{Cf}$, which are the dominant origins of the residue ^{249}Cf , almost vanish and therefore their production cross sections further drop more than 3 orders of magnitude compared with that of ^{249}Cf . In addition, we also investigate a pair of the most probable residues (^{208}Po , ^{254}Fm) of the complementary elements Po and Fm and we find that the production mechanisms of ^{208}Po and ^{254}Fm are similar to those of ^{214}Rn and ^{249}Cf ; i.e., the residual fragment ^{208}Po mainly comes from the decay of the most probable primary fragments $^{216-219}\text{Po}$ with high production probability and the residue ^{254}Fm mainly comes from the decay of more neutron-rich primary fragments $^{262-263}\text{Fm}$ by eight to nine neutrons evaporation rather than from the most probable primary Fm fragments.

Now let us study the causes of the large differences among the production cross sections for the most probable light residue ^{214}Rn , the most probable heavy residue ^{249}Cf , and the neutron-rich residues $^{254-256}\text{Cf}$, which is valuable for synthesizing neutron-rich transuranium nuclei. It is well known that fission and neutron evaporation are two main competition processes in the decay of light uraniumlike and transuranium primary fragments. The competition of these two processes can possibly produce different features in producing light uraniumlike and heavy transuranium products. To understand the results shown in Figs. 4 and 5 we further investigate the isotope dependence of the average excitation energies (E^*) of primary fragments for the corresponding elements with the ImQMD model. The calculation of the neutron evaporation width and the fission barrier height B_f are already included in the HIVAP code. The neutron evaporation width increases with the neutron number increasing with a small stagger from the pairing effect in the mass number region $A = 240-270$ for Cf, Es, and Fm at a fixed excitation energy. However, the isotope dependence of the fission barrier height for these elements is more complicated. Figure 6 shows the isotope dependence of the average excitation energies of primary fragments (upper panels) and the fission barrier heights (lower panels) for the elements Rn, Cf, Es, and Fm. Figures 6(a)–6(d) indicate that the average excitation energies of primary fragments generally decrease with an increase in mass number. The average excitation energy of the most probable primary fragment ^{222}Rn is lower than the average excitation energies of transuranium fragments Cf, Es, Fm, etc. Figures 6(e)–6(h) show that the most probable residual fragments ^{214}Rn and ^{249}Cf are all located near the local peaks of the isotope distributions. It helps those fragments survive from fission. Moreover, the fission barrier height for Rn is much higher compared with that of Cf, so that the production cross section for residue ^{214}Rn is about 3 orders of magnitude larger than that for ^{249}Cf . It is the main reason that the cross sections for light uraniumlike fragments are much higher than those for heavy transuranium fragments. Upon looking at the isotope distributions of fission barrier heights for Cf, Es, and Fm in Figs. 6(f)–6(h) more closely, we find that the fission barrier heights first decrease from the local peak and then become flat at around $A = 253-260$, $A = 255-260$,

and $A = 256-263$ for Cf, Es, and Fm, respectively, and then decrease again after the flat part as the neutron number further increases. The primary fragments $^{255-259}\text{Cf}$ which contribute to the residue ^{249}Cf are all at the flat part (more neutron-rich side) of the isotope distribution of the fission barrier height, which means that, for the primary fragments $^{255-259}\text{Cf}$, the fission width increases more slowly with the neutron number increasing for the same excitation energy, and thus it is beneficial for the enhancement of the ratio of neutron evaporation width to fission width for the isotopes at the flat part. This is an important reason why ^{249}Cf is not from the decay of the most probable primary fragment ^{253}Cf but from more neutron-rich primary fragments $^{255-259}\text{Cf}$ besides the isotope dependence of excitation energies shown in Fig. 6(b). Following the end of the flat part, the fission barrier height decreases quickly with further increase of the neutron number and the fission rate increases rapidly, and thus the contribution of the neutron evaporation channel to the neutron-rich residues $^{254-256}\text{Cf}$ drops quickly. Based on the above discussions we can conclude that, for the production of neutron-rich transuranium nuclei, it is very important to study the behavior of the isotope distribution of the fission barrier heights for heavy transuranium nuclei, in addition to the isotope dependence of yields and average excitation energies of primary fragments of relevant elements. This investigation may help us to search the best combination of projectile and target for synthesis of new neutron-rich isotopes of heavy and superheavy nuclei by using multinucleon transfer reactions.

IV. SUMMARY

The mechanism of the production of the light uraniumlike and transuranium fragments in the reaction $^{238}\text{U} + ^{238}\text{U}$ at 7.0 MeV/nucleon is studied using the ImQMD model incorporated with the statistical evaporation model (HIVAP code). The dynamical process is described by the ImQMD model and the primary fragments are obtained at the end of the dynamical calculations. The decay of primary fragments is calculated using the HIVAP code. The production cross sections for primary and residual fragments of transuranium and their complementary uraniumlike nuclei are calculated. The cross sections for residual transuranium nuclei with $Z = 94-100$ are generally in agreement with the experimental data of $^{238}\text{U} + ^{238}\text{U}$. Our calculations show that the cross sections for the residual light fragments with $Z \leq 91$ are close to those of the primary fragments due to the high fission barrier. The cross sections for the residual transuranium fragments are several orders of magnitude smaller than those of the primary fragments due to a much lower fission barrier.

The microscopic production mechanism of the most probable light residual fragment ^{214}Rn and the most probable transuranium residual fragment ^{249}Cf , as well as the neutron-rich residues $^{254-256}\text{Cf}$, is carefully investigated. The isotope distributions of primary fragments are of the parabolic shape and it is indicated from these distributions that a large mass transfer takes place during the dynamical process of the strong dissipative reaction $^{238}\text{U} + ^{238}\text{U}$. The residual fragment ^{214}Rn mainly comes from the decay of the most probable

primary fragments of Rn through evaporating several neutrons with high production cross sections. The transuranium residue ^{249}Cf mainly comes from the decay of the more neutron-rich primary fragments $^{255}\text{--}^{259}\text{Cf}$ by evaporating six to ten neutrons rather than from the most probable primary fragment ^{253}Cf . The production cross section for ^{249}Cf is about 3 orders of magnitude lower than that for ^{214}Rn because of the much lower fission barrier. For the neutron-rich transuranium residues $^{254}\text{--}^{256}\text{Cf}$, the production cross sections further drop more than 3 orders of magnitude compared with the production cross section for ^{249}Cf because the contribution from the decay of primary Cf fragments by evaporating neutrons almost vanishes. The large difference in the production cross sections for the most probable residue ^{249}Cf and neutron-rich residues $^{254}\text{--}^{256}\text{Cf}$ is possibly related to the behavior of the isospin dependence of the fission barrier heights for Cf, in addition to the decrease of the cross sections for the neutron-rich Cf primary fragments. It suggests a careful study of the behavior of the isotope distribution of the fission barrier heights of relevant heavy transuranium nuclei. This investigation may

help us to discover the best combination of projectile and target for the synthesis of new neutron-rich isotopes of heavy and superheavy nuclei by using multinucleon transfer reactions. The study on the production probability of superheavy nuclei in $^{238}\text{U} + ^{238}\text{U}$ and other heavy nuclear systems with the present model is our next goal. The calculations are already under way.

ACKNOWLEDGMENTS

We are grateful to V. I. Zagrebaev for insightful discussion and Caiwan Shen for the help in the calculation of the HIVAP code. We also acknowledge support by the computing server C3S2 at Huzhou University. This work is supported by the National Natural Science Foundation of China under Grants (No. 11005155, No. 11275052, No. 11375062, No. 11475262, and No. 11475004) and by the National Key Basic Research Development Program of China under Grant No. 2013CB834404.

-
- [1] A. Ghiorso *et al.*, *Nucl. Phys. A* **583**, 861c (1995).
 [2] Yu. A. Lazarev *et al.*, *Phys. Rev. C* **54**, 620 (1996).
 [3] V. Ninov *et al.*, *Phys. Rev. Lett.* **83**, 1104 (1999).
 [4] Yu. Ts. Oganessian, V. K. Utyonkov, Yu. V. Lobanov *et al.*, *Phys. Rev. Lett.* **83**, 3154 (1999); *Phys. Rev. C* **63**, 011301(R) (2000); **69**, 021601 (2004); **70**, 064609 (2004); **74**, 044602 (2006).
 [5] Yu. Ts. Oganessian, V. K. Utyonkov, S. N. Dmitriev *et al.*, *Phys. Rev. C* **72**, 034611 (2005).
 [6] P. A. Ellison, K. E. Gregorich, J. S. Berryman *et al.*, *Phys. Rev. Lett.* **105**, 182701 (2010).
 [7] Yu. Ts. Oganessian, F. Sh. Abdullin, S. N. Dmitriev *et al.*, *Phys. Rev. Lett.* **108**, 022502 (2012).
 [8] Yu. Ts. Oganessian, F. Sh. Abdullin, C. Alexander *et al.*, *Phys. Rev. Lett.* **109**, 162501 (2012).
 [9] E. K. Hulet *et al.*, *Phys. Rev. Lett.* **39**, 385 (1977).
 [10] K. D. Hildenbrand, H. Freiesleben, F. Pühlhofer *et al.*, *Phys. Rev. Lett.* **39**, 1065 (1977).
 [11] M. Schädel *et al.*, *Phys. Rev. Lett.* **41**, 469 (1978).
 [12] H. Essel, K. Hartel, W. Henning *et al.*, *Z. Phys. A* **289**, 265 (1979).
 [13] H. Freiesleben, K. D. Hildenbrand, F. Pühlhofer *et al.*, *Z. Phys. A* **292**, 171 (1979).
 [14] M. Schädel *et al.*, *Phys. Rev. Lett.* **48**, 852 (1982).
 [15] K. J. Moody, D. Lee, R. B. Welch, K. E. Gregorich, G. T. Seaborg, R. W. Loughheed, and E. K. Hulet, *Phys. Rev. C* **33**, 1315 (1986).
 [16] R. B. Welch, K. J. Moody, K. E. Gregorich, D. Lee, and G. T. Seaborg, *Phys. Rev. C* **35**, 204 (1987).
 [17] V. I. Zagrebaev and W. Greiner, *J. Phys. G: Nucl. Part. Phys.* **35**, 125103 (2008).
 [18] V. I. Zagrebaev and W. Greiner, *Phys. Rev. C* **83**, 044618 (2011).
 [19] V. I. Zagrebaev, Y. T. Oganessian, M. G. Itkis, and Walter Greiner, *Phys. Rev. C* **73**, 031602(R) (2006).
 [20] V. I. Zagrebaev and W. Greiner, *J. Phys. G: Nucl. Part. Phys.* **34**, 1 (2007).
 [21] V. I. Zagrebaev and W. Greiner, *Nucl. Phys. A* **834**, 366c (2010).
 [22] V. I. Zagrebaev and W. Greiner, *Phys. Rev. C* **87**, 034608 (2013).
 [23] C. Golabek, A. C. C. Villari, S. Heinz *et al.*, *Int. J. Mod. Phys. E* **17**, 2235 (2008).
 [24] J. V. Kratz, M. Schädel, and H. W. Gäggeler, *Phys. Rev. C* **88**, 054615 (2013).
 [25] C. Riedel and W. Nörenberg, *Z. Phys. A* **290**, 385 (1979).
 [26] H. Freiesleben and J. V. Kratz, *Phys. Rep.* **106**, 1 (1984).
 [27] C. Golabek and C. Simenel, *Phys. Rev. Lett.* **103**, 042701 (2009).
 [28] D. J. Kedziora and C. Simenel, *Phys. Rev. C* **81**, 044613 (2010).
 [29] N. Wang, L. Ou, Y. Zhang, and Z. Li, *Phys. Rev. C* **89**, 064601 (2014).
 [30] N. Wang, K. Zhao, and Z. Li, *Phys. Rev. C* **90**, 054610 (2014).
 [31] K. Wen, F. Sakata, Z.-X. Li, X.-Z. Wu, Y.-X. Zhang, and S.-G. Zhou, *Phys. Rev. Lett.* **111**, 012501 (2013).
 [32] N. Wang, Z. Li, and X. Wu *et al.*, *Mod. Phys. Lett. A* **20**, 2619 (2005).
 [33] K. Zhao, Z. Li, X. Wu, and Y. Zhang, *Phys. Rev. C* **88**, 044605 (2013).
 [34] J. Tian, X. Wu, K. Zhao, Y. Zhang, and Z. Li, *Phys. Rev. C* **77**, 064603 (2008).
 [35] K. Zhao, X. Wu, and Z. Li, *Phys. Rev. C* **80**, 054607 (2009).
 [36] N. Wang, X. Wu, and Z. Li, *Phys. Rev. C* **67**, 024604 (2003).
 [37] N. Wang, Z. Li, and X. Wu, *Phys. Rev. C* **65**, 064608 (2002).
 [38] N. Wang, Z. Li, X. Wu, J. Tian, Y. Zhang, and M. Liu, *Phys. Rev. C* **69**, 034608 (2004).
 [39] P. Möller, J. R. Nix, W. D. Myers, and W. J. Swiatecki, *At. Data Nucl. Data Tables* **59**, 185 (1995).
 [40] W. Reisdorf, F. P. Hessberger, K. D. Hildenbrand *et al.*, *Nucl. Phys. A* **444**, 154 (1985).
 [41] C. Shen, G. Kosenko, and Y. Abe, *Phys. Rev. C* **66**, 061602(R) (2002).